Extended Data for:

Single-cell absolute contact probability detection reveals that chromosomes are organized by modulated stochasticity

Table of Contents

Online Methods

Oligopaint probesets

Supplementary Table 1: Oligopaint probe sets for libraries.

Chr	Lib	Genomic coordinates		Coverage (kb)	Number of oligos	Specific primer pairs	
2L	1	5265000	5285000	20	304	BB287-FWD	BB288-REV
2L	2	5320000	5340000	20	310	BB293-FWD	BB294-REV
2L	3	5520000	5550000	30	530	BB295-FWD	BB296-REV
2L	4	5715000	5745000	30	475	BB84-FWD	BB83-REV
2L	5	9990000	10010000	20	267	BB287-FWD	BB288-REV
2L	6	10180000	10210000	30	405	BB293-FWD	BB294-REV
2L	7	10420000	10540000	120	1615	BB295-FWD	BB296-REV
2L	8	10710000	10750000	40	516	BB84-FWD	BB83-REV
2L	9	10980000	11010000	30	488	BB193-FWD	BB280-REV
2L	10	11100000	11130000	30	523	BB82-FWD	BB278-REV
2L	11	11265000	11295000	30	522	BB81-FWD	BB281-REV
2L	12	11500000	11530000	30	480	BB298-FWD	BB187-REV
2L	13	12995000	13025000	30	30	AB_12-FWD	AB_13-REV
3R	14	12260000	12330000	70	944	BB291-FWD	BB292-REV
3R	15	12450000	12480000	30	405	BB300-FWD	BB301-REV
3R	16	12840000	12960000	120	1541	BB302-FWD	BB303-REV
2L	IT-17	10065000	10095000	30	482	BB291-FWD	BB292-REV
2L	IT-18	10265000	10295000	30	479	BB300-FWD	BB301-REV
2L	IT-19	10600000	10630000	30	462	BB302-FWD	BB303-REV

PCR primers and secondary oligonucleotides

Fluorophore-labelled PCR primers, 5'-phosphorylated PCR primers used in the lambda exonuclease protocol and DNA secondary oligos purified by using high-performance liquid chromatography were purchased from IDT (Coralville, US) . Unlabelled, unphosphorylated primers purified by using standard desalting, were also purchased from IDT.

Supplementary Tables 2-4 display the list of PCR primer pairs and secondary oligos used in this work.

Supplementary Table 2: Unlabelled PCR primers

Name	Sequence	Lib	Chr
BB287-FWD	/5Phos/CGCTCGGTCTCCGTTCGTCTC	1	2L
Sec1-BB288-REV	CACCGACGTCGCATAGAACGGAAGAGCGTGTGGGGCTAGGTACAGGGTTCAGC	1	2L
BB293-FWD	/5Phos/CCGAGTCTAGCGTCTCCTCTG	2	2L
Sec1-BB294-REV	CACCGACGTCGCATAGAACGGAAGAGCGTGTGAACAGAGCCAGCCTCTACCTG	2	2L
Sec5-BB294-REV	TAGCGCAGGAGGTCCACGACGTGCAAGGGTGTAACAGAGCCAGCCTCTACCTG	2	2L
BB295-FWD	/5Phos/GCGTTAGGGTGCTTACGTCTG	3	2L
Sec1-BB296-REV	CACCGACGTCGCATAGAACGGAAGAGCGTGTGCACCTCCGTCTCTCACCTCTC	3	2L
Sec5-BB296-REV	TAGCGCAGGAGGTCCACGACGTGCAAGGGTGTCACCTCCGTCTCTCACCTCTC	3	2L
BB84-FWD	/5Phos/GATACGTTGGGAGGCAATGAG	4	2L
Sec1-BB83-REV	CACCGACGTCGCATAGAACGGAAGAGCGTGTGATCCTAACAATCCCGCTGAGG	4	2L
Sec5-BB83-REV	TAGCGCAGGAGGTCCACGACGTGCAAGGGTGTATCCTAACAATCCCGCTGAGG	4	2L
BB287-FWD	/5Phos/CGCTCGGTCTCCGTTCGTCTC	5	2L
Sec1-BB288-REV	CACCGACGTCGCATAGAACGGAAGAGCGTGTGGGGCTAGGTACAGGGTTCAGC	5	2L
BB293-FWD	/5Phos/CCGAGTCTAGCGTCTCCTCTG	6	2L
Sec1-BB294-REV	CACCGACGTCGCATAGAACGGAAGAGCGTGTGAACAGAGCCAGCCTCTACCTG	6	2L
Sec5-BB294-REV	TAGCGCAGGAGGTCCACGACGTGCAAGGGTGTAACAGAGCCAGCCTCTACCTG	6	2L
BB295-FWD	/5Phos/GCGTTAGGGTGCTTACGTCTG	7	2L
Sec1-BB296-REV	CACCGACGTCGCATAGAACGGAAGAGCGTGTGCACCTCCGTCTCTCACCTCTC	7	2L
Sec5-BB296-REV	TAGCGCAGGAGGTCCACGACGTGCAAGGGTGTCACCTCCGTCTCTCACCTCTC	7	2L
BB84-FWD	/5Phos/GATACGTTGGGAGGCAATGAG	8	2L
Sec1-BB83-REV	CACCGACGTCGCATAGAACGGAAGAGCGTGTGATCCTAACAATCCCGCTGAGG	8	2L
Sec5-BB83-REV	TAGCGCAGGAGGTCCACGACGTGCAAGGGTGTATCCTAACAATCCCGCTGAGG	8	2L
BB193-FWD	/5Phos/TTGATCTCGCTGGATCGTTCT	9	2L
Sec5-BB280-REV	TAGCGCAGGAGGTCCACGACGTGCAAGGGTGTGGGAGTAGGGTCCTTTGTGTG	9	2L
BB82-FWD	/5Phos/GTATCGTGCAAGGGTGAATGC	10	2L
Sec1-BB278-REV	CACCGACGTCGCATAGAACGGAAGAGCGTGTGGAGCAGTCACAGTCCAGAAGG	10	2L

BB81-FWD	/5Phos/ATCCTAGCCCATACGGCAATG	11	2L
Sec5-BB281-REV	TAGCGCAGGAGGTCCACGACGTGCAAGGGTGTGGACATGGGTCAGGTAGGTTG	11	2L
BB298-FWD	/5Phos/CGTCAGTACAGGGTGTGATGC	12	2L
Sec1-BB187-REV	CACCGACGTCGCATAGAACGGAAGAGCGTGTGTTGATCTTGACCCATCGAAGC	12	2L
AB_12-FWD	/5Phos/TCGGCCCTTATCGGTAGCAG	13	2L
Sec1-AB_13-REV	CACCGACGTCGCATAGAACGGAAGAGCGTGTGCAACGCGCTCGTGTACAACG	13	2L
BB291-FWD	/5Phos/CAGGTCGAGCCCTGTAGTACG	14	3R
Sec1-BB292-REV	CACCGACGTCGCATAGAACGGAAGAGCGTGTGCTAGGAGACAGCCTCGGACAC	14	3R
BB300-FWD	/5Phos/CCAGTGCTCGTGTGAGAAGTC	15	3R
Sec1-BB301-REV	CACCGACGTCGCATAGAACGGAAGAGCGTGTGCTGCAGAGAAGAGGCAGGTTC	15	3R
Sec5-BB301-REV	TAGCGCAGGAGGTCCACGACGTGCAAGGGTGTCTGCAGAGAAGAGGCAGGTTC	15	3R
BB302-FWD	/5Phos/CGCACTGAACCAGACTACCTG	16	3R
Sec1-BB303-REV	CACCGACGTCGCATAGAACGGAAGAGCGTGTGGAGAGGCGAGGACACCTACAG	16	3R
Sec5-BB303-REV	TAGCGCAGGAGGTCCACGACGTGCAAGGGTGTGAGAGGCGAGGACACCTACAG	16	3R
BB291-FWD	/5Phos/CAGGTCGAGCCCTGTAGTACG	17	2L
Sec1-BB292-REV	CACCGACGTCGCATAGAACGGAAGAGCGTGTGCTAGGAGACAGCCTCGGACAC	17	2L
BB300-FWD	/5Phos/CCAGTGCTCGTGTGAGAAGTC	18	2L
Sec1-BB301-REV	CACCGACGTCGCATAGAACGGAAGAGCGTGTGCTGCAGAGAAGAGGCAGGTTC	18	2L
Sec5-BB301-REV	TAGCGCAGGAGGTCCACGACGTGCAAGGGTGTCTGCAGAGAAGAGGCAGGTTC	18	2L
BB302-FWD	/5Phos/CGCACTGAACCAGACTACCTG	19	2L
Sec1-BB303-REV	CACCGACGTCGCATAGAACGGAAGAGCGTGTGGAGAGGCGAGGACACCTACAG	19	2L
Sec5-BB303-REV	TAGCGCAGGAGGTCCACGACGTGCAAGGGTGTGAGAGGCGAGGACACCTACAG	19	2L

Supplementary Table 3: Labelled PCR primers

Name	Sequence
BB506-A647 (Sec1)	/5Alex647N/CACCGACGTCGCATAGAACGG
BB506-A488 (Sec1)	/5Alex488N/CACCGACGTCGCATAGAACGG
BB510-Cy3B (Sec5)	/5Cy3B/TAGCGCAGGAGGTCCACGAC

Supplementary Table 4: Secondary labelled oligos

Name	Sequence
Sec1-A647-X2(Sec1)	/5Alex647N/CACACGCTCTTCCGTTCTATGCGACGTCGGTGagatgttt/3AlexF647N/
Sec1-A488-X2(Sec1)	/5Alex488N/CACACGCTCTTCCGTTCTATGCGACGTCGGTGagatgttt/3AlexF488N/
Sec5-Cy3B-X2(Sec5)	/5Cy3B/ACACCCTTGCACGTCGTGGACCTCCTGCGCTAagatgttt/3Cy3B/

Emulsion PCR amplification of oligonucleotide libraries

Raw, multiplexed libraries purchased from CustomArray were amplified using emulsion PCR with universal primers (forward primer : GACTGGTACTCGCGTGACTTG and reverse primer : GTAGGGACACCTCTGGACTGG) to generate templates employed in the subsequent PCR reactions. Set up a 100µl PCR Master mix (80µl H2O, 10µl 10X Taq buffer, 5µl BSA at 10µg/µl, 2µl dNTP at 10mM, 0.5µl FWD primer at 200µM, 0.5µl REV primer at 200µM, 1µl Taq DNA polymerase, 1µl ssDNA library at 20ng/µl) for each library, and keep on ice until needed. Vortex a 50 ml stock tube of oil phase (95.95% mineral oil (Sigma M5904):4% ABIL EM90 (Degussa):0.05% Triton-X-100 (Sigma T8787) oil phase (v/v/v)) to mix it. Remove a pre-chilled 2ml glass vial (VWR 66009-822) from the -20°C freezer and place on the center of a controlled stir plate. Add a fresh stir bar (BelArt 371191083) to the vial. Use a positive displacement pipette to transfer 600µl mixed oil phase to the glass vial and stir at 1000 rpm for >1 minute. With the stir bar still spinning, add 100µl of PCR master mix previously prepared in 20 µl increments using a p20 (i.e. dispense 20µl 5 times). Stir at 1000 rpm for 10 minutes (the emulsion should appear milky white and foamy). Stop the stir plate and use a positive displacement pipette to transfer the emulsion to a PCR strip tube (~8 x 75µl). Run the following PCR program: 95°C for 2 min then 30 cycles of 1)95°C for 15sec, 2)60°C for 15s, 3)72°C for 20s then final step 72°C for 5 min.The quality of the emulsion can be monitored by taking a 10-15 µl aliquot of the mixed emulsion and placing it on a microscope slide (the emulsion droplets should have a median diameter of 8-10 µM). After cycling, the DNA was recovered by a series of organic extractions: first using diethyl ether (Sigma 296082), then using ethyl acetate (Sigma 494518); then once again using diethyl ether. These extractions were followed by a purification of DNA samples with Qiagen columns to remove Taq polymerase. For stepwise emulsion, PCR and emulsion breaking protocols, please see the Oligopaints website (http://genetics.med.havard.edu/oligopaints).

Oligopaint probe synthesis

Oligopaints probes containing secondary oligo binding sites were synthesized using the lambda exonuclease method [1]. The secondary oligo-binding sites were added to Oligopaint probe sets through the use of the following 'touch-up' PCR cycle: 95 C for 5min; 3 cycles of 95 °C for 30 s, 60 °C for 45 s and 72 °C for 30 s; 20 cycles of 95 °C for 30 s, 68 °C for 1min and 72 °C for 30 s, with a final extension step at 72 °C for 5min. The template generated via 'touch-up' PCR was further amplified with the following cycle: 95 °C for 5min; 31 cycles of 95 °C for 30 s, 60 °C for 30 s and 72 °C for 15 s, with a final extension step at 72 °C for 5min. For stepwise probe synthesis protocols, please see the Oligopaint website (http://genetics.med.havard.edu/oligopaints).

'One-day' probe synthesis using lambda exonuclease

Oligopaint probe sets were amplified using the 'two-PCR' method described above, but with the unlabeled primer being phosphorylated on its 5'end. The PCR reaction was then collected, concentrated using spin columns (Zymo D4031) and digested with lambda exonuclease (New England Biolabs M0262). Five units of lambda exonuclease were added per every 100 ml of unconcentrated PCR reaction (for example, use 50 units if the labelling PCR had a volume of 1 ml before concentration by the spin column) and the reaction was incubated at 37 °C for 30 min in a thermocycler and then stopped by incubation at 75 °C for 10 min. Finally, the digestion products were concentrated using ethanol precipitation and quantified using Nanodrop. For a detailed protocol, please see the OligoPAINT website (http://genetics.med.havard.edu/oligopaints).

ModEncode data files used in this study

A description of the genome-wide ChIP-chip/seq data files used for assignment of chromatin state is provided in Supplementary Table 5.

Supplementary Table 5: ChIP-chip/seq data files employed in this study

Cell type	Epigenetic mark	File ID
Late Embryo	*H3K4me3*	modENCODE_5096
	H3K27me3	modENCODE_3955
	PC	modENCODE_3957
Early Embryo	*H3K4me3*	modENCODE_789
	H3K27me3	modENCODE_3811
	PC	modENCODE_5064
S2	*H3K4me3*	modENCODE_914
	H3K27me3	modENCODE_298
	PC	modENCODE_326

Correlation of replicates of late-embryo and S2 Hi-C interaction maps

Supplementary Table 6: Correlation of Hi-C replicates

Mapping fly data [date: june'16; enzyme: DpnII; genome: dm3]

Experiment	Read	Reads	Mapped	%	Mapped Int.	%	Valid int.	%	Dangling	Extra DE	Duplicates	R. breaks	Over rep.	Error	Self circle	Final merged valid int.
Late embryo replicate 1	1	771,584,699	543,089,230	70.4 %												
	2	771,584,699	523,164,711	67.8 %	461,642,603	59.8 %	113,867,043	14.8 %	189,398,549	41 % 50,386,592	11 % 222,013,421	48 % 122,332,379	26 % 6,873,614	1 % 132,479	0 % 1,068,660	0 %
Late embryo replicate 2	1	765,716,879	503,352,249	65.7 %												
	2	765,716,879	479,743,113	62.7 %	416,797,286	54.4 %	168,158,279	22.0 %	131,890,044	32 % 18,994,806	5 % 109,469,472	26 % 112,554,684	67 % 6,499,838	2 % 128,892	0 % 413,190	0 % 282,025,322
S2 replicate 1	1	619,637,214	449,119,241	72.5 %												
	2	619,637,214	437,937,471	70.7 %	382,574,953	61.7 %	92,244,799	14.9 %	166,503,128	44 % 24,627,012	6 % 158,379,607	41 % 137,160,088	36 % 9,403,744	2 % 560,411	0 % 1,570,343	0 %
S2 replicate 2	1	768,189,050	473,607,172	61.7 %												
	2	768,189,050	464,792,365	60.5 %	415,009,752	54.0 %	38,522,335	5.0 %	231,820,094	56 % 91,873,204	22 % 271,699,414	65 % 114,735,347	298 % 8,462,059	2 % 377,255	0 % 632,010	0 %
S2 replicate 3	1	440,441,503	287,855,072	65.4 %												
	2	440,441,503	281,915,992	64.0 %	225,500,438	51.2 %	79,568,795	18.1 %	69,733,515	31 % 7,648,210	3 % 69,269,233	30 % 70,259,409	88 % 4,916,355	2 % 401,564	0 % 202,378	0 % 210,335,929

Supplementary Figures

Figure S1

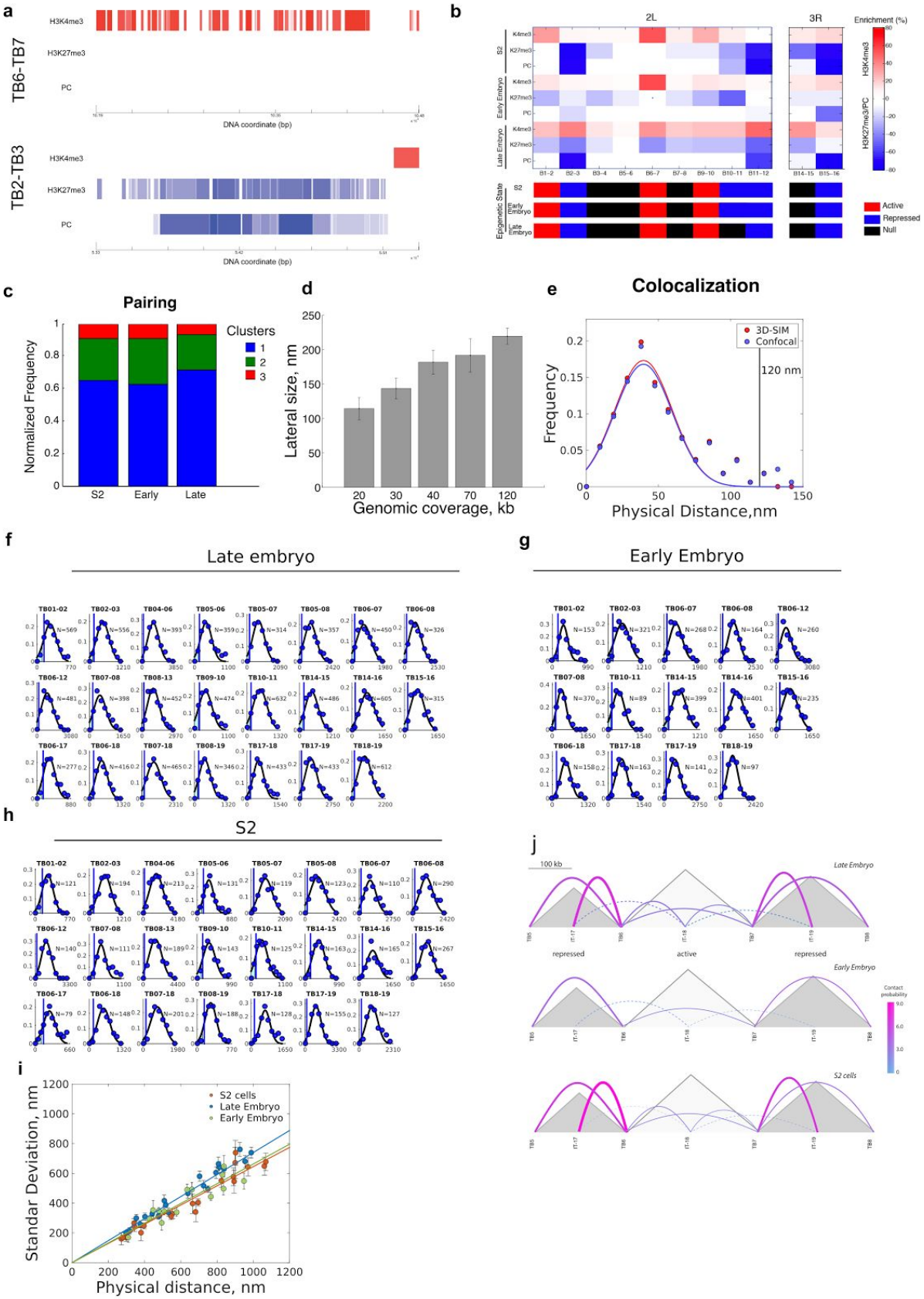

(a-b) Classification of TADs chromatin states. **(a)** shows representative examples of active (top) and repressed (bottom) chromatin states. Chip-Seq profiles for H3K4me3 (red), H3K27me3 (blue) and Polycomb (PC, blue) for TADs between borders TB6-TB7 and TB2-TB3 (upper and lower panels) are depicted. Abscissas indicate the genomic coordinates between the barriers. Color intensities in Chip-seq profiles are proportional to intensity of the detected peak according to the color-coded scale on the right. **(b)** Upper panel shows the total enrichment for each mark between barriers for each cell type employed in this work calculated as defined in the paragraph below. Colorcode in scale bar on the right is proportional to the percentage of H3K4me3 (red), H3K27me3 (blue) and PC (blue). Lower panel depicts the resulting chromatin state of each TAD depending on the proportions of each epigenetic mark (see paragraph below 'Definition of chromatin states') defining active (red), inactive (black) and repressed (blue) chromatin states. ChIP-chip/seq computed peaks were downloaded from ModEncode (ftp://data.modencode.org/D.melanogaster/) and datasets used are described in Supplementary Table 5.

Definition of chromatin states

Epigenetic states of TADs encompassed between consecutive oligoPAINT libraries were classified into three categories: active, inactive and repressed, based on enrichment of histone modifications and Polycomb from ChIP-seq profiles for each cell type (early embryonic, late embryonic and S2 cells) obtained from the modENCODE database [2]. Active chromatin TADs were selected based on the enrichment of histone modifications H3K4me3. Repressed TADs were selected based on the enrichment of H3K27me3 and/or Polycomb (PC) proteins. Inactive TADs were selected based on the total or partial depletion of H3K4me3, H3K27me3 and PC proteins. In each case the percentage of enrichment for each mark was calculated as the ratio between the number of base pairs bound by each epigenetic mark over the total number of base pairs between consecutive libraries. Domains containing more than 25% of a given mark and less than 25% of the remaining marks were considered as enriched for that particular mark (*e.g.* region between TB1 and TB2 for S2 cells displays H3K4me3 = 34%, H3K27me3= 3%, PC = 0, then the region is defined as enriched for H3K4me3 and defined as active TAD). Regions having less than 25% enrichment for any mark were considered as inactive. To confirm our results, enrichment for marks in each region was also visually inspected using a homemade Matlab routine and Gbrowse (GBrowse.org).

(c) Homologous pairing for the different cell types. We estimated the pairing of chromosomes by counting the total number of foci detected for each Oligopaint library per single cell from 3D-SIM imaging. Pairing was similar for all cells types and above 60%. For simplicity the population average for all libraries is displayed. Y coordinates indicate the relative frequency of detection of foci while the x coordinates indicates the type of cell line analyzed. A total of 5130, 1310 and 1882 cells were computed for the analysis in late embryo, early embryo and S2 cells, respectively. We note that early and late embryonic cells are diploid, while S2 cells present typically four copies of each chromosome (Zhang et al. 2010).

(d) Population average lateral size of foci as a function of the genomic size of the 19 oligopaint libraries employed in this work.

(e) Distribution of distances for TAD border TB2 labelled in two colors and imaged either by confocal microscopy or by 3D-SIM. Both distributions are identical with median and standard deviation of 42 and 26 nm, respectively. The black solid line at 120 nm includes >99% of total observations. N = 161 and N = 166 for 3D-SIM and confocal microscopy measurements, respectively. From these experiments, we calculate the precision of localization in our measurements at 40 nm and define that any two TAD borders located at less than 120 nm are co-localizing.

Note on the colocalization precision in 3D-SIM and the selected threshold to calculate absolute contact probability.

Colocalization between multicolor fluorescent beads yields the maximal precision of colocalization that can be measured, in our conditions, by 3D-SIM for isotropic objects of sizes smaller than the resolution limit and located at the surface of the coverslip when imaged in two distinct channels (colocalization = 30 ± 5 nm, mean ± SD). This value, that reveals the minimal distance at which two objects can be considered as colocalizing, is rather ideal and arises from bright objects located at the surface of the coverslip. Thus, it does not take into account the effect of low signal and background noise and depth-dependent spherical aberrations introduced for objects further away from the objective. To determine the precision of colocalization between libraries and to emulate an equivalent situation to that employed for all libraries imaged in this work, we fluorescently labelled the same library with two spectrally-different fluorophores and measured their separating distance. In our experimental conditions the minimal distance that indicates that two libraries colocalize is (42 ± 26 nm, mean ± SD, i.e. a co-localization precision 30%

lower than in ideal conditions). In a conservative approach, we decided to employ the results obtained from a single library labelled with two colors and the upper limit of the distribution obtained to measure the absolute probability of contact between borders. Then from the Gaussian fitting we assume that two libraries have 99% chances of co-localizing if their separating distances is less than 120 nm (i.e. three standard deviations away from the mean).

Increasing the distance threshold to calculate contact probability does not increase significantly the measured frequency of interaction.

Contacts detected through chromosome conformation capture techniques such as Hi-C can be located in the 3D space at distances ranging from tens to a few hundreds of nanometers [5]. To ensure that the low probability of contacts between borders obtained with our method was not due to a selection of threshold that could underestimate the mapped distances by Hi-C, we increased systematically the value of the threshold starting at 100 nm in steps of 50 nm. For all the values tested the probabilities increased as expected but remained low reaching (18.2±2.6%, mean±SEM) in average for the largest threshold of 300 nm.

(f-h) Distribution of distances for all pairs of libraries computed in this work for late (**f**) and early (**g**) embryos, and for S2 cells (**h**). In all panels, the Y axis indicates the relative frequency while the X axis indicates the physical distances measured. A Gaussian fit (black line) was used to determine the mean and standard deviation. Blue vertical solid lines represent the colocalization threshold (120 nm) for a single library labelled with two colors with a 99% confidence interval as described in Fig. S1e. Light blue shaded area indicates the integral under the curve for each gaussian fitting to calculate the absolute contact probability. The number of each pair of libraries computed is indicated on top of each panel and N represents the number of cells analyzed from at least three biological replicates.

(i) To get further insight into the mechanism of chromatin folding within epigenetic domains, the standard deviation of distance measurements between barriers was plotted as a function of the mean physical distance between borders for all three cell types. Notably, the relation between these quantities was linear and independent of chromatin type for all cell types. Note that the slope was slightly higher for late embryo than for early embryo and S2 cells (0.74 ± 0.03, 0.66 ± 0.05, 0.65 ± 0.03 nm/nm, respectively), indicating that for equivalent mean size of TADs their structure

display higher dynamics in late embryonic cells. Error bars represent the standard error of the mean (SEM) as obtained from bootstrapping.

(j) Schematic representation of contact probability between and within TADs (solid colored lines) as depicted in the main figure for late embryo and S2 cells and including early embryo (middle panel). Size of triangles representing TADs (grey shaded) is proportional to genomic length (scale bar on top). Chromatin type is indicated at the bottom of each TAD. Thickness of the lines is proportional to the absolute contact probability with values depicted in color coded scale bar on the right. Dotted lines indicate inter-TADs contact probabilities.

Figure S2

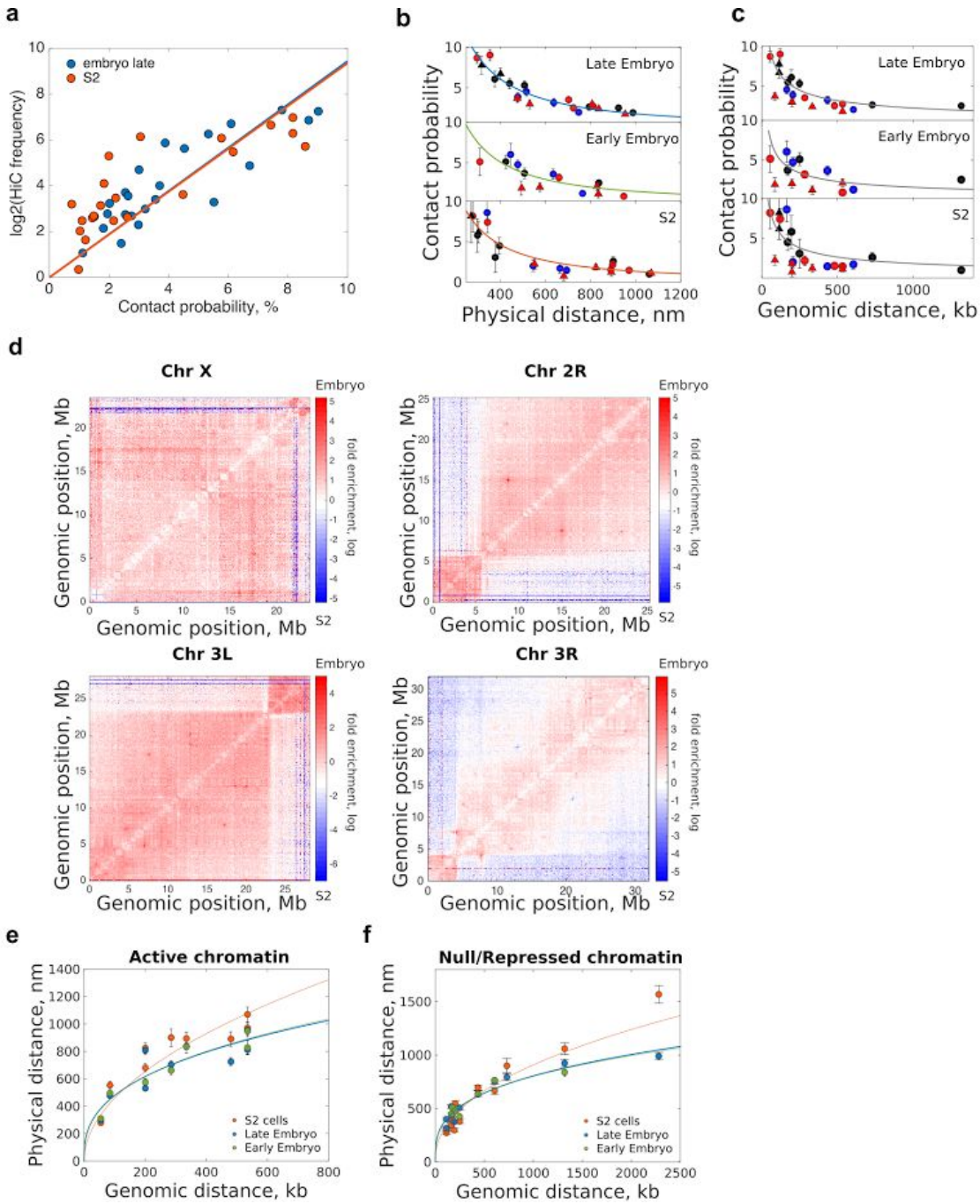

(a) Log_2 Hi-C contact frequency *vs.* microscopy absolute contact probability for consecutive and non-consecutive TAD borders for embryo (light blue) and S2 cells (orange). Blue and orange line represent a linear fitting for late embryo and S2 cells. Note that both cell types display equivalent non-linear relations between Hi-C and microscopy measurements.

(b) Absolute contact probabilities as a function of physical distance for consecutive and non-consecutive TAD borders for late embryo, early embryo and S2 cells. Chromatin

state of domains encompassed by borders is color-coded as defined in Figs. S1b and S1a-b. Error bars represent the standard error of the mean (SEM) as obtained from bootstrapping. Circles are employed when the pair of libraries are at borders and triangles are employed when at least one of the libraries is within a TAD. Experimental data was best described by a power-law $P = \alpha\, d_{3D}^{-\theta}$ (solid lines reproducing color code of Fig. 2b of the main text). The pre-factor α was obtained from the best fitting parameters values of late embryo (α = $1.6E^4$) and kept constant for the other fittings. The scaling exponent best fitting values were: ***θ*** = 1.31 ± 0.01, ***θ*** = 1.35 ± 0.03, ***θ*** = 1.36 ± 0.02 for late embryo, early embryo and S2 cells, respectively.

(c) Absolute contact probabilities as a function of genomic distance with chromatin state colors and symbols as in Fig. S2b. Solid lines are a guide-to-the-eye. Note that given the different degree of compaction between chromatin states (see Figs. 2e-f and S2d), for equivalent genomic distances the contact probability for active chromatin is systematically lower than that of inactive/repressed chromatin domains.

(d) Matrix of relative frequency of Hi-C contacts for late embryo *vs.* S2 cells for chromosomes X, 2R, 3L, and 3R. Scale Bar represents the logarithmic ratio of the contact frequencies between cell types. Resolution=50 kb.

(e-f) Plots of mean physical distance between pairs of oligopaints libraries flanking active **(e)** or inactive/repressed chromatin **(f)** as a function of genomic distance. The lines indicate a power-law fitting ($d_{3D} = \gamma d_{kb}^{\beta}$), with the exponent ***β*** as displayed in Fig 2e-f. The pre-exponential factors were **ɣ**=88 ± 25, **ɣ**=93 ±35 and **ɣ**=41 ± 25 for late embryo, early embryo and S2 cells, respectively. Circles are employed when the pair of libraries are at barriers while triangles are employed when at least one of the libraries is within a TAD. Error bars represent ± SEM.

Figure S3

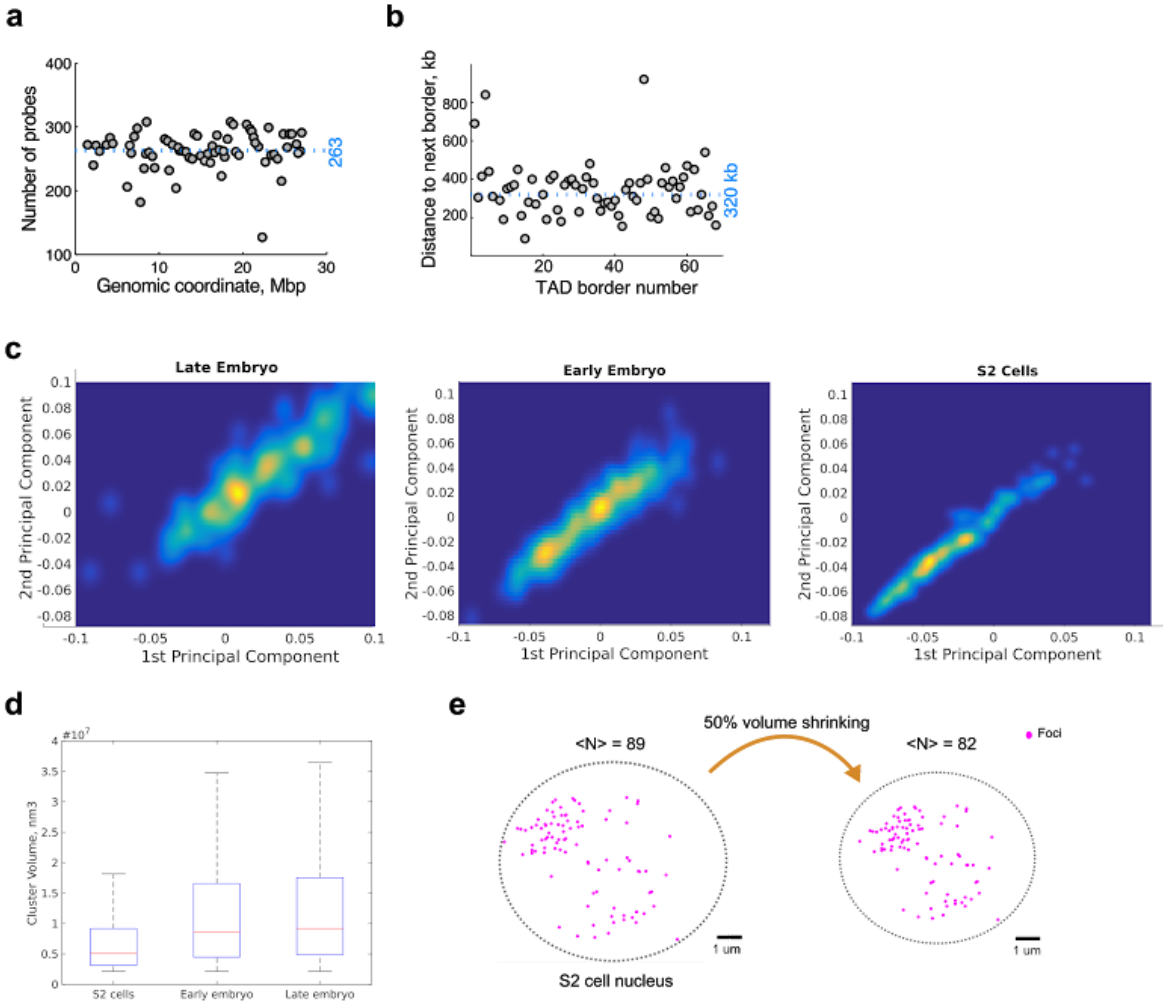

(a) Total number of probes used for each library as a function of the genomic coordinate. The average number of probes is 263.

(b) Genomic distance between consecutive TAD borders as a function of border number. Barriers are numbered sequentially from centromere to telomere. The distribution of distances between barriers is homogeneous, with a mean of 320 kb.

(c) Principal component analysis of *p(r)* distributions.

(d) Average size of foci detected from simultaneously labelling 69 barriers in chromosome 3R. Note that the volume per foci increases from S2 cells to early and late embryo respectively, consistent with data shown in Fig. 3.

(e) The lower number of detected foci in embryonic cells is not associated with their reduced nucleus volume with respect to S2 cells. Left, clusters detected after segmentation of a representative S2 cell. Right, same cell after volume shrinkage of 50%. <N> indicates the average number of clusters detected before and after nucleus volume reduction for a representative cell. The difference in detected number of

cluster cannot account for the differences observed between cell types. To test more quantitatively if the reduced number of clusters observed in embryonic cells was due to the reduced nucleus volume of embrionyc cells (50% reduction with respect to S2 cells) combined with the inability of 3D-SIM to resolve foci separated by distances below the resolution limit (~120 nm in xy, ~250 nm in z), we computationally reduced the total volume occupied by all foci in S2 cells. To this end, the radial distance of all detected foci respect to the center of mass was reduced by 20% (equivalent to a 50% reduction in volume in a perfect sphere) and next we quantified the number of foci that remained at a distance resolvable by 3D-SIM. The number of foci detected after volume shrinking diminished by less than ~7%. The latter confirms that the lower number of detected foci in early and late embryos arises from a higher frequency of interaction between TAD borders and not from the smaller volume of cells or limitations in the resolutive power of 3D-SIM.

Detailed R_g and D_{max} values from Figure 3b of the main text.

	Rg	Dmax
Late embryo	1600±300	4000±9000
Early embryo	1900±300	4900±1000
S2 cells	2600±400	6400±900

Discussion on the total number of foci imaged when labelling 69 TAD borders in 3D-SIM

The total number of barriers appearing as foci in microscopy imaging can be estimated as $N = 69 \times \sum_{k=1}^{3} (p_k \times k)$, where p_k represents the relative frequency of cells displaying k foci. From the pairing frequency obtained from single border labelling (Fig. S1c) and assuming the absence of long-range interactions between TADs borders, the predicted number of foci for each cell type is 76, 90 and 90 for late embryo, early embryo and S2 cells, respectively. Our imaging results show an average of 89 ± 28 clusters per cell for S2 cell line (Fig. 3b in the main text), consistent with a very low frequency of looping between TAD borders. Interestingly, the number of foci was drastically reduced in embryonic cells (51 ± 20 for early and 36 ± 13 for late embryos, Fig. 3b of the main text). Given that the difference in total nucleus volume could not account for the lower number of observed foci (Fig. S3e), the reduction and the increase in the overall volume per foci (Fig. S3d) suggest the associated recruitment of several TAD borders in embryonic cells.

Figure S4

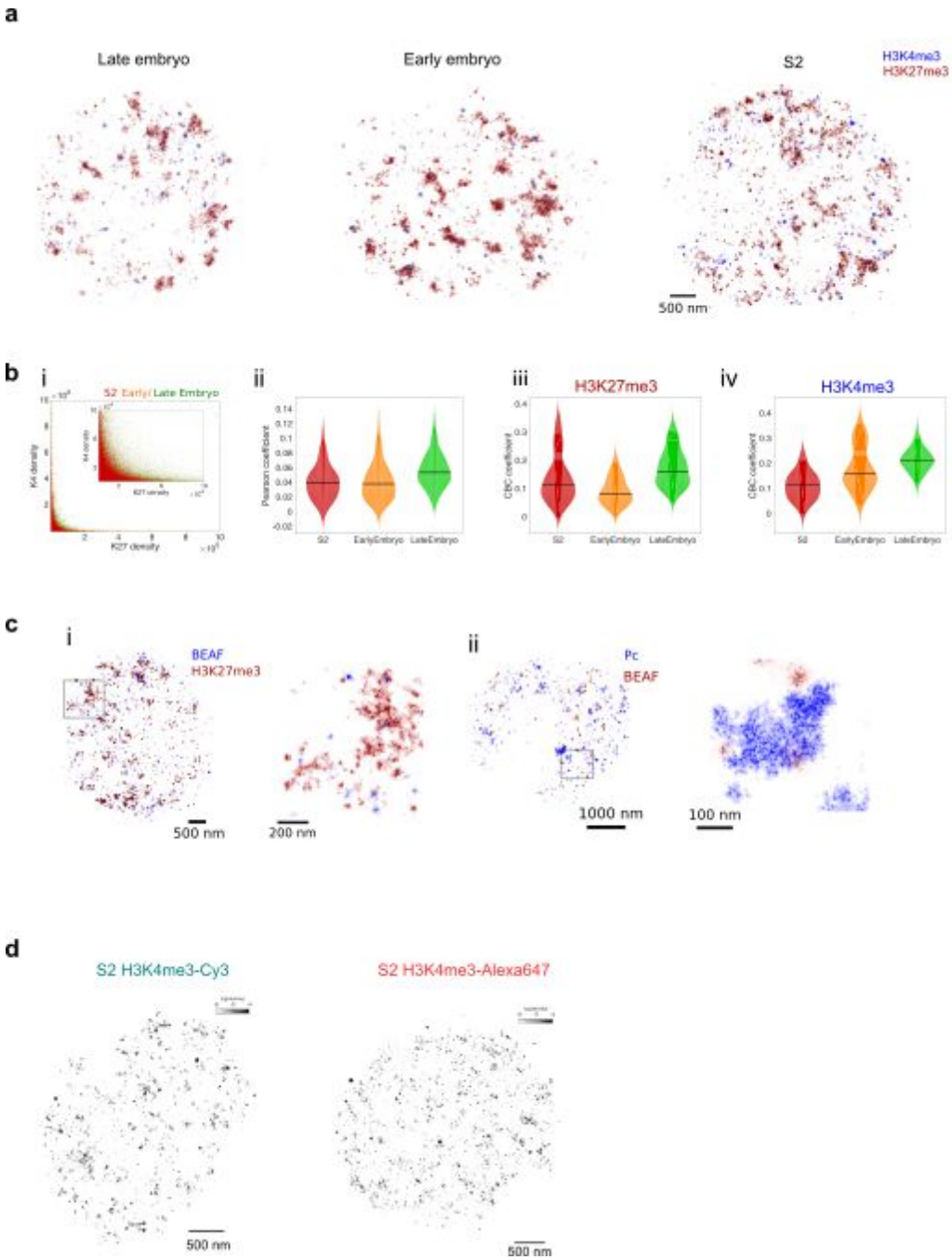

(a) Two-color dSTORM image of active (H3K4me3) and repressive (H3K27me3) chromatin marks in representative late embryo, early embryo and S2 cells.

(b) (i) Pixel-by-pixel colocalization analysis between active and repressed histone marks. The data distribution into two separate groups, showing varying signal levels of one mark with little or no signal from the other, indicates a very low level of colocalization between single molecule events. (ii) Quantification of co-occurrence between active and repressive chromatin compartments using the Pearson's colocalization

coefficients criteria for S2, early and late embryonic cells. (iii-iv) Coordinate-based colocalization analysis (CBC, [6]) of single-molecule localization images between H3K27me3 with respect to H3K4me3 events (iii) and between H3K4me3 with respect to H3K27me3 events (iv). Note that for all type of analysis active and repressed marks display very low overlap for all cell types (Pearsons coefficient < 0.1, coordinate-based coefficient (CBC) < 0.25).

(c) (i) Representative two-color dSTORM image of Beaf-32 (blue) and H3K27me3 (red) in a S2 cell. Inset on the right is a magnification of the region selected by the gray square. Beaf-32 rarely colocalizes with H3K27me3 marks. (ii) Typical two-color dSTORM image of Polycomb (blue) and Beaf-32 (red). Beaf-32 does not colocalize with Polycomb. Quantification of the degree of co-localization of Beaf-32 vs. H3K27me3 and Polycomb using single molecule colocalization analysis (CBC, [6] yielded values of 0.23 ± 0.04 and 0.18 ± 0.04 respectively, confirming the absence of colocalization between this marks.

(d) Representative comparison of single-color dSTORM imaging of H3K4me3 labelled with antibodies bearing different organic fluorophores (either Cy3 or Alexa 647, N=35). No significant differences in the spatial localization, distribution of sizes and densities of compartments were observed.

Figure S5

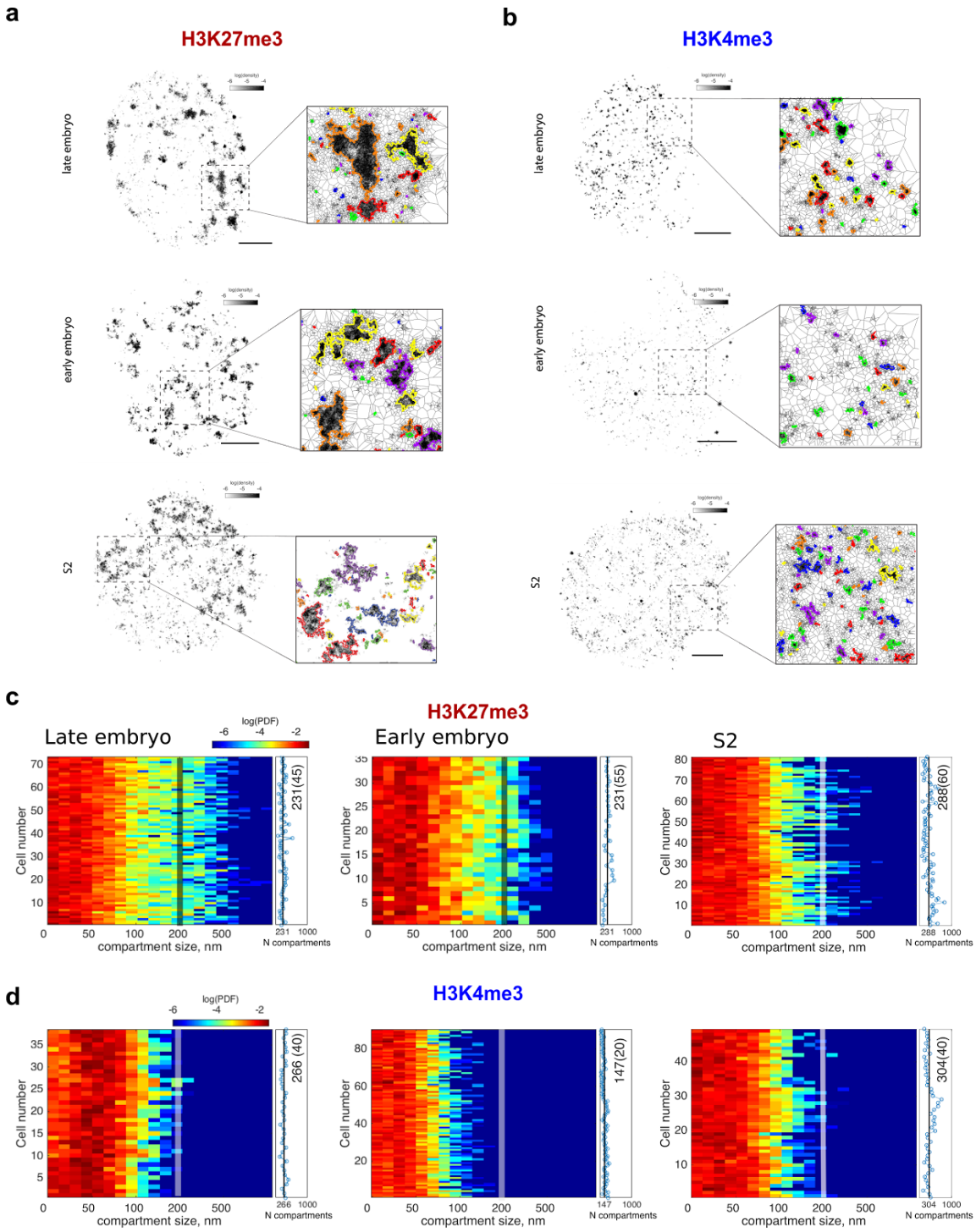

(a-b) Representative dSTORM images of Alexa-647 labelled H3K27me3 **(a)** and H3K4me3 **(b)** for all cell types employed in this work. Images show density maps computed from the area of the polygons obtained from the Voronoï diagram with color-coded scale defined at the top. Scalebar = 1 µm. Zoomed regions displaying

detected domains (highlighted with different colors) using automatic segmentation on the basis first-rank density criteria as defined in [7].

(c-d) Single cell distribution of H3K27me3 **(c)** and H3K4me3 **(d)** compartment sizes, defined as equivalent diameters in nm, for late and early embryonic and S2 cells. Each horizontal line represent the distribution from a single cell. Vertical lines at 200 nm are used as a reference to compare different histograms. Note that x-scale and colormap are in logarithmic scales (see colorbar above). Right panel to each distribution shows the number of compartments detected per cell. The mean is displayed as a vertical black line and the value and its standard deviation (in parenthesis) are quoted.

Figure S6

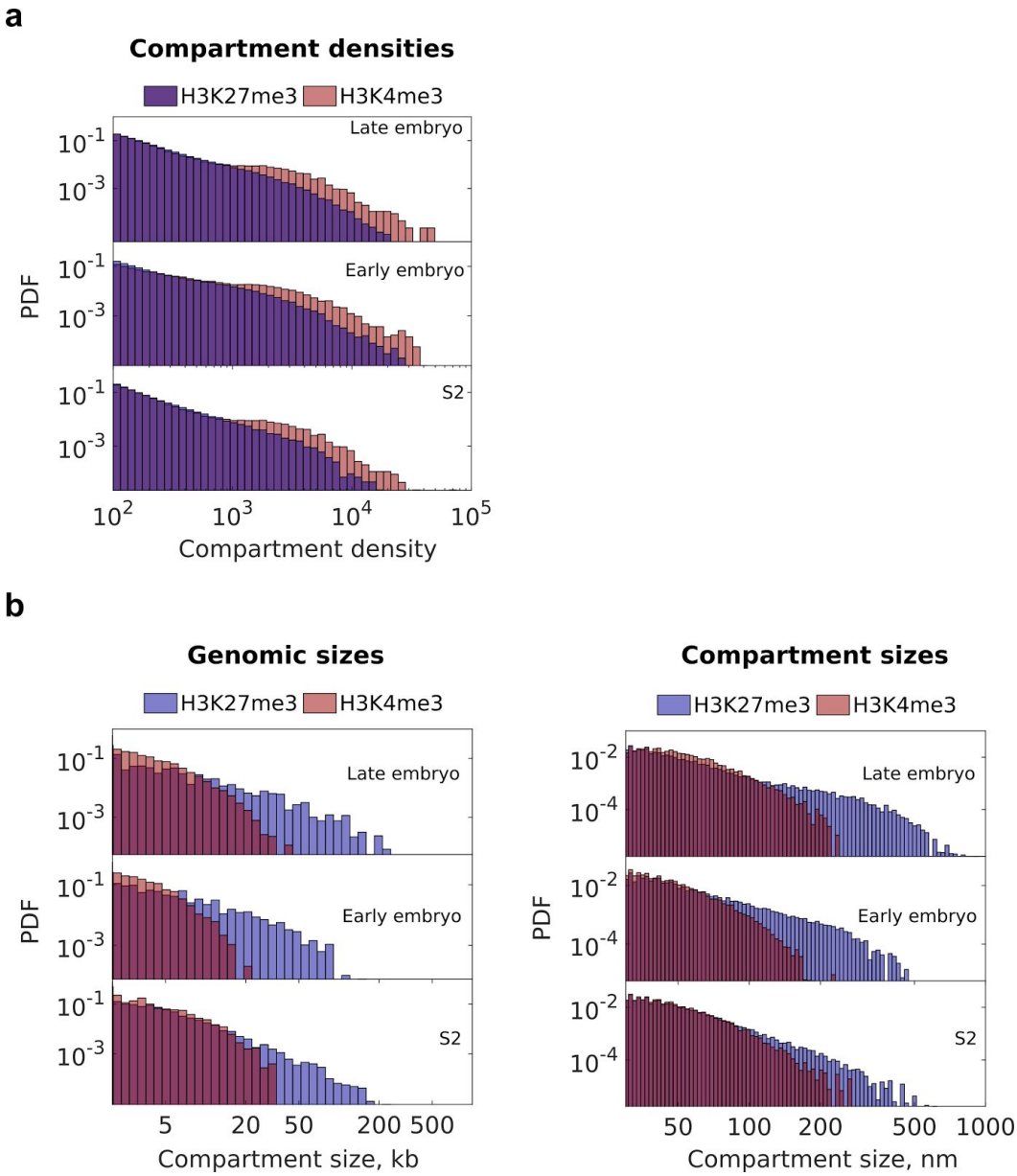

(a) Population based distribution of compartments densities for H3K4me3 and H3K27me3 chromatin marks for all cell types studied in this work. Compartment density is defined as the number of single-molecule detections divided for the area of the compartment. PDF is probability density function. Note that for all cell types, repressed mark compartments display higher densities than active compartments in good agreement with local chromatin folding measurements (see Fig. 2e-f in the main text). The density of compartments, both active and repressed, is higher in embryonic cells with respect to S2 cells, in good agreement with local chromatin folding data (Fig. 2e-f).

(b) Comparison between the ensemble distributions of genomic ChIP-Seq data (i) and dSTORM compartment physical sizes (ii) from H3K4me3 and H3K27me3 for all three cell-types analyzed. PDF is probability density function. The size distributions of repressed and active compartments were broad and stretched over several decades independently of cell type, with repressed compartments being systematically larger than active compartments. Repressed compartments were significantly larger in late embryos than in S2 cells, with early embryos displaying an intermediate behavior (panel b, right). In contrast, genomic distributions of repressive domains detected by chromatin immunoprecipitation methods [8] were similar for late embryos and S2 and smaller for early embryos (panel b,left), suggesting cell-specific clustering of epigenetic domains depending on developmental and transcriptional state of each cell type.

References

1. Beliveau, B. J. *et al.* Single-molecule super-resolution imaging of chromosomes and in situ haplotype visualization using Oligopaint FISH probes. *Nat. Commun.* **6,** 1–13 (2015).
2. Celniker, S. E. *et al.* Unlocking the secrets of the genome. *Nature* **459,** 927–930 (2009).
3. Zhang, Y. *et al.* Expression in aneuploid Drosophila S2 cells. *PLoS Biol.* **8,** e1000320 (2010).
4. Fung, J. C., Marshall, W. F., Dernburg, A., Agard, D. A. & Sedat, J. W. Homologous chromosome pairing in Drosophila melanogaster proceeds through multiple independent initiations. *J. Cell Biol.* **141,** 5–20 (1998).
5. Giorgetti, L. & Heard, E. Closing the loop: 3C versus DNA FISH. *Genome Biol.* **17,** 215 (2016).
6. Georgieva, M. *et al.* Nanometer resolved single-molecule colocalization of nuclear factors by two-color super resolution microscopy imaging. *Methods* doi:10.1016/j.ymeth.2016.03.029
7. Levet, F. *et al.* SR-Tesseler: a method to segment and quantify localization-based super-resolution microscopy data. *Nat. Methods* **12,** 1065–1071 (2015).
8. Kharchenko, P. V. *et al.* Comprehensive analysis of the chromatin landscape in Drosophila melanogaster. *Nature* **471,** 480–485 (2011).